Experimental and Theoretical Characterization of Short H–Bonds with Organic Fluorine in Molecular Crystals

ARTICLE *in* CRYSTAL GROWTH & DESIGN · MAY 2014

Impact Factor: 4.89 · DOI: 10.1021/cg5004758

2 AUTHORS:

Piyush Panini
Indian Institute of Science Education and Res…
21 PUBLICATIONS **162** CITATIONS
SEE PROFILE

Deepak Chopra
Indian Institute of Science Education and Res…
181 PUBLICATIONS **1,114** CITATIONS
SEE PROFILE

CRYSTAL GROWTH & DESIGN

Communication

pubs.acs.org/crystal

Experimental and Theoretical Characterization of Short H-Bonds with Organic Fluorine in Molecular Crystals

Piyush Panini[†] and Deepak Chopra*[,†]

[†]Department of Chemistry, Indian Institute of Science Education and Research Bhopal, Madhya Pradesh, India 462066

Supporting Information

ABSTRACT: The existence of short H-bonds with organic fluorine is still under debate. We report herein the occurrence and nature of such short contacts to fluorine connected to an aromatic ring in the block form of *N*-(4-fluorophenyl)-3-(trifluoromethyl) benzamide and 4-fluoro-*N*-[3-(trifluoromethyl)phenyl]benzamide. The magnitude of the stabilizing interaction energy is −2.15 and −2.89 kcal/mol, respectively. It is important to note that such contacts have been observed in the presence of strong N—H···O═C H-bonds whose energies are in the range of 6.0−8.0 kcal/mol. Thus, the observed strength of an H-bond with fluorine is ∼30−40% of the strength of a strong traditional H-bond in amides. The acidic hydrogens were observed to be involved in the formation of a short C—H···F contact, the interaction energy having a substantial Coulombic contribution in comparison to the other weak interactions which are primarily of a dispersive character as obtained by PIXEL method. A full topological analysis does establish the fact that C—H···F interactions at short distances are indeed a "true H-bond". These are not a consequence of crystal packing and have implications in the generation of polymorphs in the solid state. This is expected to have implications in the binding of a ligand (organic molecule containing fluorine) with the protein active site.

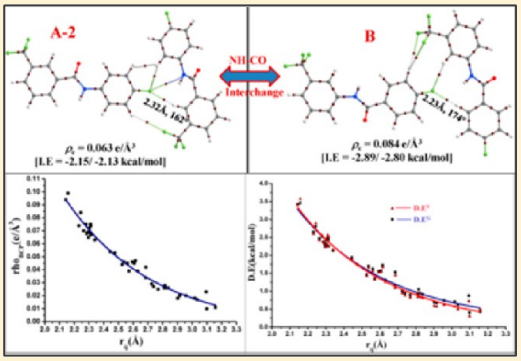

INTRODUCTION

The prevalence of noncovalent interactions is central to chemistry and biology.[1] Conventional H-bonds are well understood,[2] but the role of weak intermolecular interactions is still being explored. C—H···O/N/C interactions have already been classified as H-bonds.[3] The role of halogens, in particular, organic fluorine, in the formation of weak H-bonds has been questioned.[4] On the contrary, interactions involving organic fluorine have been observed in a large number of organic molecules. The geometrical characteristics of such interactions have been highlighted in the investigation of crystal structures of fluorobenzenes[5a,b] and ribonucleic acids.[5c] In addition, detailed reviews,[6a] highlights,[6b] and books[6c] speak about the significance of organic fluorine. A recent review emphasizes the significance of hydrogen bonds with fluorine in solution, in the gas phase, and in the crystal environment.[6d] The question that arises is whether these interactions are a consequence of other strong H-bonds or these have a definite contribution in terms of stability and their role in crystal packing. It was initially envisioned that such weak contacts would evolve only in the absence of strong H-bonds.[7] However, the synthesis of a large number of halogenated benzanilides (∼200 in number),[8] particularly containing fluorine atom,[8a] halogens,[8b] or trifluoromethyl group,[8c] connected to the phenyl rings, followed by a detailed analysis of their crystal structures have provided a significant indication of the existence of relatively short and directional C—H···F interactions. This has resulted in the generation of polymorphs in fluorinated benzanilides,[9] and these have also been observed during *in situ* crystallization of liquids,[10] containing strong H-bond donors as well. Hence, a detailed evaluation of the energetics associated with such interactions (of the type C—H···F, C—F···π, C—F···F—C) is of importance. The current work is directed toward a quantitative understanding of the energetics and the related topological properties of these weak interactions using the approach of quantum theory of atoms in molecules.[11]

In the current investigation, we have synthesized a library of molecules (18 in number) containing an amide functional group, aromatic ring connected to organic fluorine, and trifluoromethyl group separately (present in drugs and pharmaceuticals[12] (Scheme 1), so as to observe the occurrence of C—H···F—C(sp^2)/F—C(sp^3) contacts acting in conjunction with strong N—H···O═C H-bonds and related weak interactions.

Scheme 1

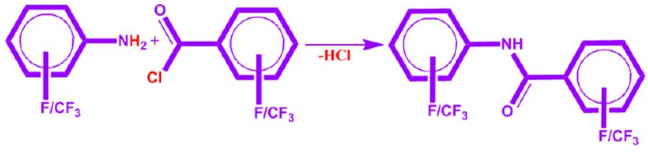

Received: February 5, 2014
Revised: May 15, 2014

   dx.doi.org/10.1021/cg5004758 | *Cryst. Growth Des.* XXXX, XXX, XXX−XXX

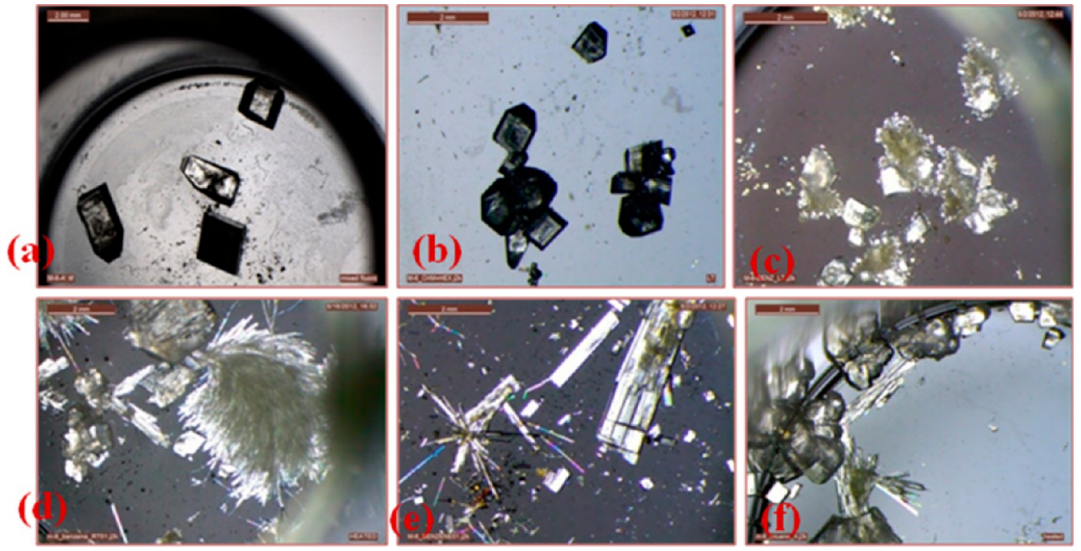

Figure 1. Crystal photos obtained by crystallization from (a) DCM + hexane at low temperature (LT) (Blocks, **A-2**). (b) Chloroform + hexane at LT (Blocks, **A-2**). (c) Benzene at LT (Blocks, **A-2**). (d) Benzene at RT (Concomitance observed on slight warming, Blocks + thin long plates [**A-1**]). (e) Benzene after heating for some time, cooling, and crystallized from RT (Plates: Same **A-1**). (f) Toluene crystallized at RT (concomitance again observed on slight warming; both forms are present).

From this library of molecules (Supporting Information section S1), a closer inspection of the crystal structures revealed significant geometrical features. The compound *N*-(4-fluorophenyl)-3-(trifluoromethyl) benzamide (**A**) exists in two polymorphic forms (**A-1** (Plate) and **A-2** (Block), Figure 1) both crystallizing in a rare combination of non-centrosymmetric space groups (orthorhombic $Pna2_1$ and monoclinic *Cc*, respectively) (Supporting Information section S2) whereas the related isomer (can be viewed as NH—CO interchange) 4-fluoro-*N*-[3-(trifluoromethyl)phenyl] benzamide (**B**) exists in a centrosymmetric form (monoclinic $P2_1/c$) only (Table 1).

EXPERIMENTAL SECTION

Synthetic procedures for the compounds (**A**) and (**B**) are given in the Supporting Information along with their yields and melting points. Scheme 1 describes the general route for the synthesis of the compounds. The compounds were characterized by FTIR (Supporting Information Figure S1a–b) and ^{1}H NMR (Supporting Information Figure S2a–b) spectroscopy.

Crystal Growth, Single Crystal Data Collection, and Structure Solution. The crystallization experiments by slow evaporation technique were performed on the synthesized compounds by dissolving them in different solvents or solvent mixtures (DCM + hexane, chloroform + hexane, acetone + hexane, acetonitrile + hexane, ethyl acetate + hexane, toluene, benzene, and so forth) at low temperature in a refrigerator maintained at 5 °C and also at RT. This results in the generation of crystals of two different morphologies (plates and blocks) for compound **A** (Figure 1). The details of the crystallization results are presented in Supporting Information Table S1. Single crystal X-ray diffraction experiments and related characterizations (Figures 2–5) confirmed the formation of two polymorphs for compound **A**. In further discussions, these are named **A-1** (Plate) and **A-2** (Block). Compound **B** crystallizes in only one form (rod-like crystals). Crystals from all possible solvents and solvent combinations were screened for new polymorphs, but none were obtained.

Single crystal X-ray diffraction data of **A-1** and **A-2** were collected on CrysAlis CCD Xcalibur, Eos (Nova), Oxford Diffraction, with an X-ray generator operating at 50 kV and 1 mA, using Mo Kα radiation (λ = 0.7107 Å)[13] at 120 K. Single crystal X-ray diffraction data of **B** was collected on a Bruker AXS SMART APEX II CCD Diffractometer at 100 K. All the crystal structures were solved by direct methods using SIR 92[14] and refined by the full matrix least-squares method using SHELXL97[15] present in the program suite WinGX.[16] ORTEP of all the compounds were generated using ORTEP32[17] (Figure 6) and packing diagrams were generated using Mercury software.[18] The crystallographic and refinement data are given in Table 1. Selected torsion angles in **A-1**, **A-2**, and **B** are presented in Table 2.

Table 1. Crystallographic and Refinement Data

data	A-1	A-2	B
formula	$C_{14}H_9NOF_4$	$C_{14}H_9NOF_4$	$C_{14}H_9NOF_4$
formula weight	283.22	283.22	283.22
solvent	benzene (heated, RT)	DCM + hexane, 5 °C	DCM + hexane, 5 °C
CCDC no.	981 078	981 077	981 079
crystal system; space group	Orthorhombic; $Pna2_1$	Monoclinic; *Cc*	Monoclinic; $P2_1/c$
a (Å)	9.4513(3)	14.2784(10)	10.7039(18)
b (Å)	13.6988(15)	11.3734(9)	12.496(2)
c (Å)	9.4512(9)	14.8822(11)	8.8106(15)
α (°)/ β (°)/ γ (°)	90/90/90	90/96.670(4)/ 90	90/92.281(3)/ 90
volume/density (g/cm^3)	1223.66(18)/ 1.537	2400.4(3)/ 1.567	1177.6(3)/ 1.598
Z/*Z*′	4/1	8/2	4/1
F (000)/ μ (mm^{-1})	576/0.139	1152/0.142	576/0.144
θ (min, max)	2.97, 30.72	2.30, 30.53	1.90, 25.00
$h_{min,max}$, $k_{min,max}$, $l_{min,max}$	−12, 13; −19, 19; −13, 9	−20, 19; −16, 16; −21, 21	−12, 11; −12, 14; −10, 10
no. of ref.	18 981	24 129	5840
no. unique ref./ obs. ref.	2609, 1924	7110, 6469	2079, 1987
no. of parameters	217	433	217
R_all, R_obs	0.0643, 0.0420	0.0403, 0.0349	0.0331, 0.0316
wR_2_all, wR_2_obs	0.0808, 0.0759	0.0830, 0.0802	0.0779, 0.0768
$\Delta\rho_{min,max}$(eÅ^{-3})	−0.195, 0.195	−0.203, 0.318	−0.279, 0.189
G.o.F	0.921	1.038	1.074

Characterization of Polymorphs of *N*-(4-Fluorophenyl)-3-(trifluoromethyl)benzamide (A). The two polymorphs have been characterized using differential scanning calorimetry (DSC), hot stage microscopy (HSM), Fourier transform infrared spectroscopy (FTIR), and powder X-ray diffraction (PXRD) techniques (Figures 2–5).

dx.doi.org/10.1021/cg5004758 | *Cryst. Growth Des.* XXXX, XXX, XXX–XXX

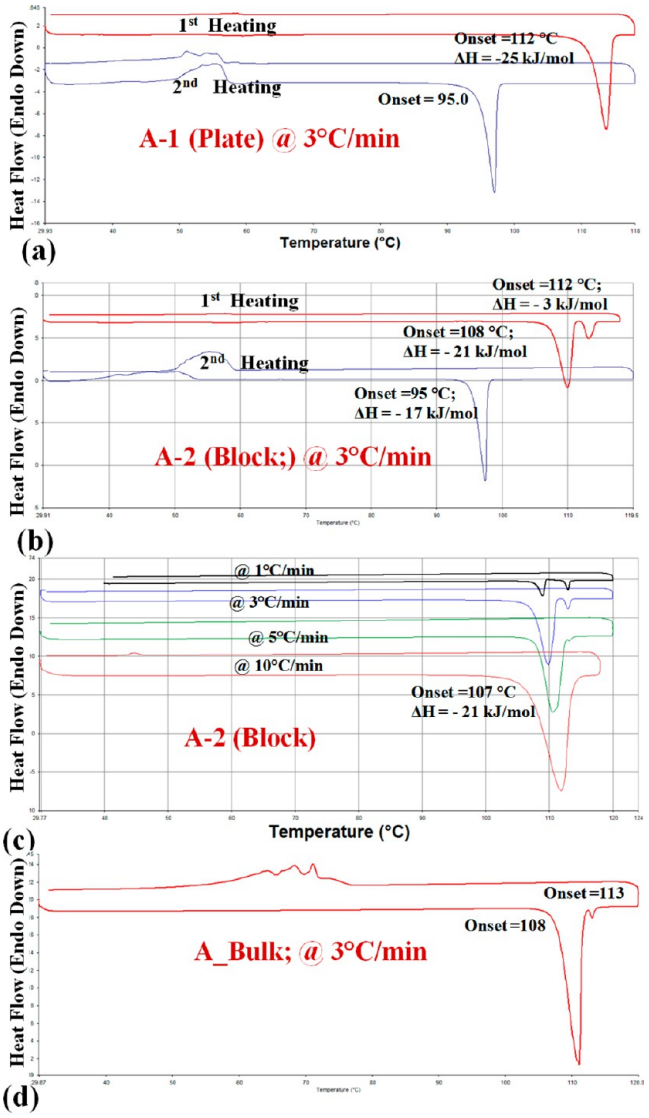

Figure 2. DSC traces of (a) Plate form of A (**A-1**) @ 3 °C/min of 2 heating−cooling cycles. (b) Block form of A (**A-2**) @ 3 °C/min of two heating−cooling cycle; (c) **A-2** at different heating rate; (d) **A_bulk** @ 3 °C/min.

DSC experiments were performed on the bulk powder and the two polymorphs of **A** with PerkinElmer DSC 6000 instrument (Figure 2). The results suggest the presence of a small endothermic peak for melting of **A-1** at 112 °C (ΔH_t = −25 kJ/mol) and no phase transition is detected during the first heating cycle (Figure 2a). In the subsequent heating cycle an endothermic peak at 95.0 °C may suggest its transition to some other metastable phase after melting. However, DSC traces for **A-2** displays endothermic peaks: the two are near to each other [first: 108 °C (ΔH_t = −21 kJ/mol); second: 112 °C (ΔH_t = −3.0 kJ/mol); scanning rate 3 °C/min; Figure 2b]. To characterize these transitions, DSC experiments with different scanning rates (Figure 2c) have been performed. DSC traces for different heating rates suggest that the second peak becomes more prominent with reduction of the scan rate while slowly disappearing at high scan rates. With scanning rate of 10 °C/min, the second endothermic peak disappears completely, hence could be considered as melting of **A-2** (107 °C; ΔH_t = −21 kJ/mol) without transition to another phase. By looking at the transition temperature in the DSC traces for the slower scanning rate, it indicates that there exists the possibility of a phase transition of **A-2** (Block form) to **A-1** (Plate form). To verify this, the hot stage microscopy experiment (HSM) has been performed on Linkam LTS420 heating and freezing stage system (Figure 3). Images were collected with a Leica polarizing microscope. The snapshots of the experiment confirm that the melting of **A-1** (Plate) occurs without any transition while **A-2** displays transition to plate form (scanning rate of 0.5 °C/min) at 107.7 °C, followed by melting of plate form (**A-1**) at 112.2 °C. Both DSC and HSM experiments (Figures 2b and 3b) on **A-2** show transition to a metastable form after melting in the first heating cycle at 95 °C (ΔH_t = −17 kJ/mol).

Comparison of the experimental powder pattern of the bulk powder (collected on Phillips X-ray powder diffractometer equipped with X'lerator detector) with the simulated PXRD pattern (Figure 4a) shows that the bulk is representative of **A-2** (Block form). The profile fitting refinement was performed by JANA2000[19] on the experimental powder pattern of the bulk compound with the lattice parameters for the block form (**A-2**) (Figure 5a) and then including the lattice parameters for the plate form (**A-1**) (Figure 5b). The results suggests that the bulk powder is mainly present as **A-2** (block form).

By comparison of IR spectra of bulk powder with those of **A-1** and **A-2**, we see the blue shift in N—H and C═O stretching frequencies (45 and 5 cm^{-1}, respectively) for **A-1**, while IR spectrum of **A-2** appears to match with that of **A_Bulk** (Figure 4b).

Computational Tools and Theoretical Calculations. The lattice energy with its breakdown into Coulombic, polarization, dispersion, and repulsion contributions was calculated for all the structures (Table 3) with PIXELC module in the CLP computer program package (version 10.2.2012).[20] For this purpose hydrogen atoms were moved to their neutron values and an accurate electron density of the molecules were obtained at MP2/6-31G** with Gaussian 09.[21] The interaction energies of the selected molecular pairs (from mlc file after PIXEL calculation), extracted from the crystal packing along with the involved intermolecular interactions, were listed in Table 4 with the total energies being partitioned into their Coulombic, polarization, dispersion, and repulsion contributions. The total energies for the molecular pair, obtained from the PIXEL method, were also compared with counterpoise corrected[22] stabilization energies calculated by the DFT+Disp/B97-D method (Supporting Information Table S2) with higher aug-cc-pVTZ basis set using JOBBSSE script in Turbomole.[23] The calculation with the DFT-D/B97-D method has been performed only for comparison of interaction energy (on the basis of our previous studies and also because this method is computationally inexpensive and results are similar to those from the MP2 method[24]) calculated from the PIXEL-method and have not been included in the discussion. The results obtained from PIXEL calculation were found to be comparable with high level MP2 and DFT-D quantum mechanical calculations in the literature.[25]

Analysis of Topological Parameters. The *ab initio* calculation for the selected dimers at the crystal geometry, with the hydrogen atoms moved to their neutral value, was performed at the MP2/6-311G** level of theory (with "density = current" keyword) using Gaussian 09. Then, the formatted checkpoint file (fchk) was considered for the input for AIMALL (version 13.05.06),[26] which was then used to generate the wave function file (.wfx file) by the software itself and followed by the topological analysis. The selected topological parameters like electron densities (ρ_c), Laplacian ($\nabla^2\rho_c$), local potential energy (V_b), and kinetic energy density (G_b) at the bond critical points (BCPs) were calculated. The dissociation energies for the different intermolecular interactions were also estimated through the following two empirical approaches: (i) $D.E^V(int) = -0.5\ V_b$ (in atomic units)[27] and (ii) $D.E^G(int) = -0.429\ G_b$ (in atomic units);[28] where D.E(int) is the dissociation energy of the interaction. Interaction energy (I.E) = −D.E. V_b and G_b are local potential and kinetic energy density at the bond critical points (BCPs), respectively.

Equation (i) had been suggested mainly for weak or moderate hydrogen bonds ($d_{H\cdots O}$ > 1.60 Å and E_{HB} < 60 kJ/mol) and were used to estimate the interaction energy for C—H···O hydrogen bonds.[27a] However, this was also used to estimate interaction energies of other related weak noncovalent interactions.[27b,c] This equation was also used in the evaluation of interaction energies in H_2O−Serine and H_2O_2−Serine complexes for N/O—H···O hydrogen bond.[27d] Recently, Wolstenholme and co-workers estimated the strength of N—$H^{\delta+}\cdots^{\delta-}$H—B, C—H···H—C, and B—$H^{\delta-}\cdots^{\delta+}$H—B interactions using equation (i).[27e,f]

dx.doi.org/10.1021/cg5004758 | Cryst. Growth Des. XXXX, XXX, XXX−XXX

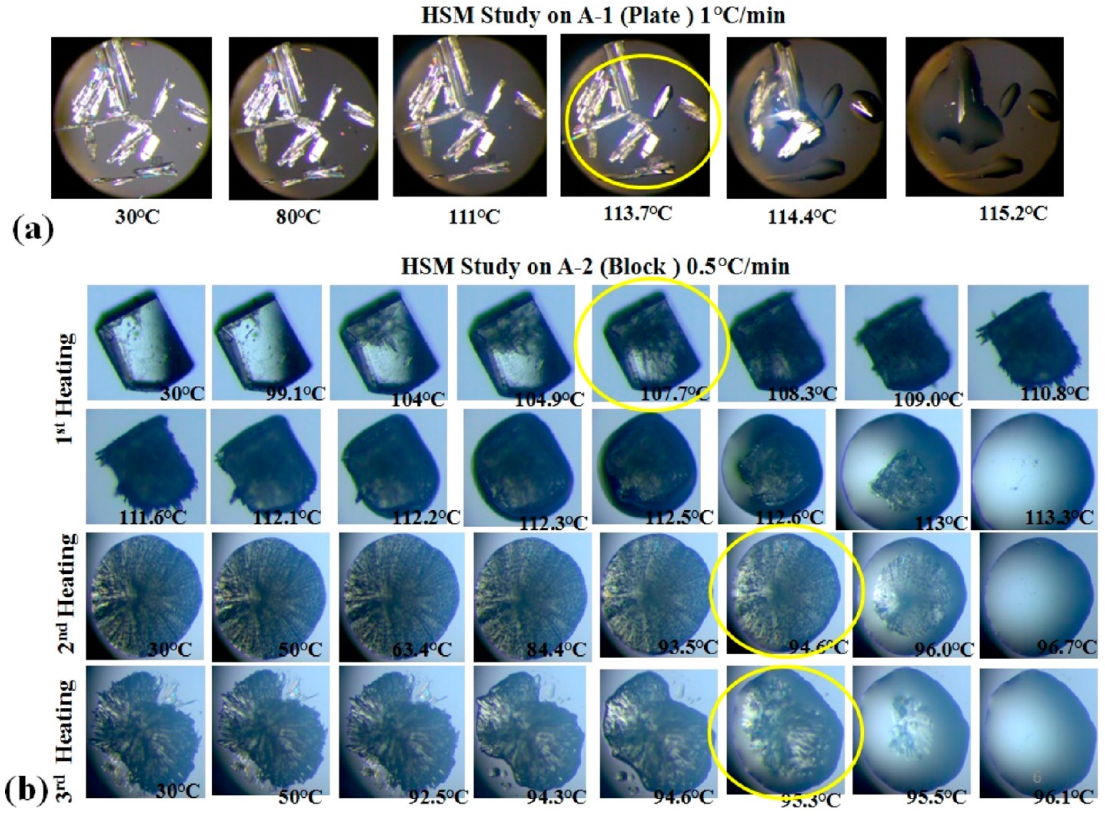

Figure 3. HSM snapshots for (a) **A-1** and (b) **A-2**. Yellow circles indicate the starting point of the phase transition.

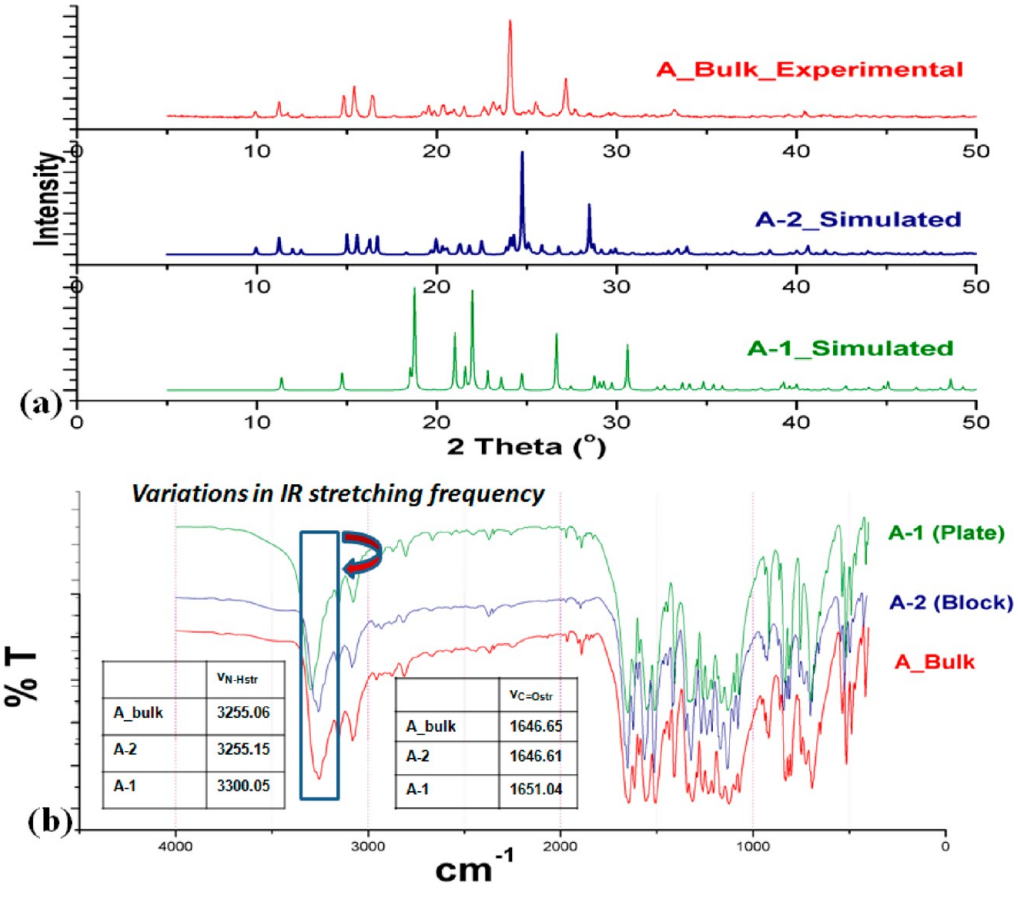

Figure 4. Overlay of (a) PXRD pattern and (b) IR spectra of **A_Bulk**, **A-1**, and **A-2**.

dx.doi.org/10.1021/cg5004758 | *Cryst. Growth Des.* XXXX, XXX, XXX−XXX

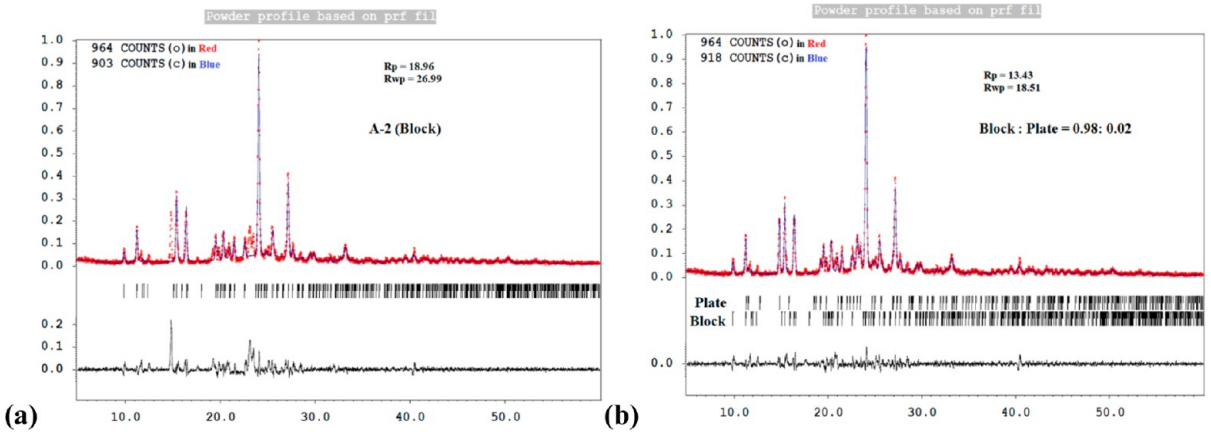

Figure 5. (a,b) Profile fitting refinement was performed with JANA 2000[19] for polymorphs of compound **A** with the experimental powder pattern for the bulk compound **A**.

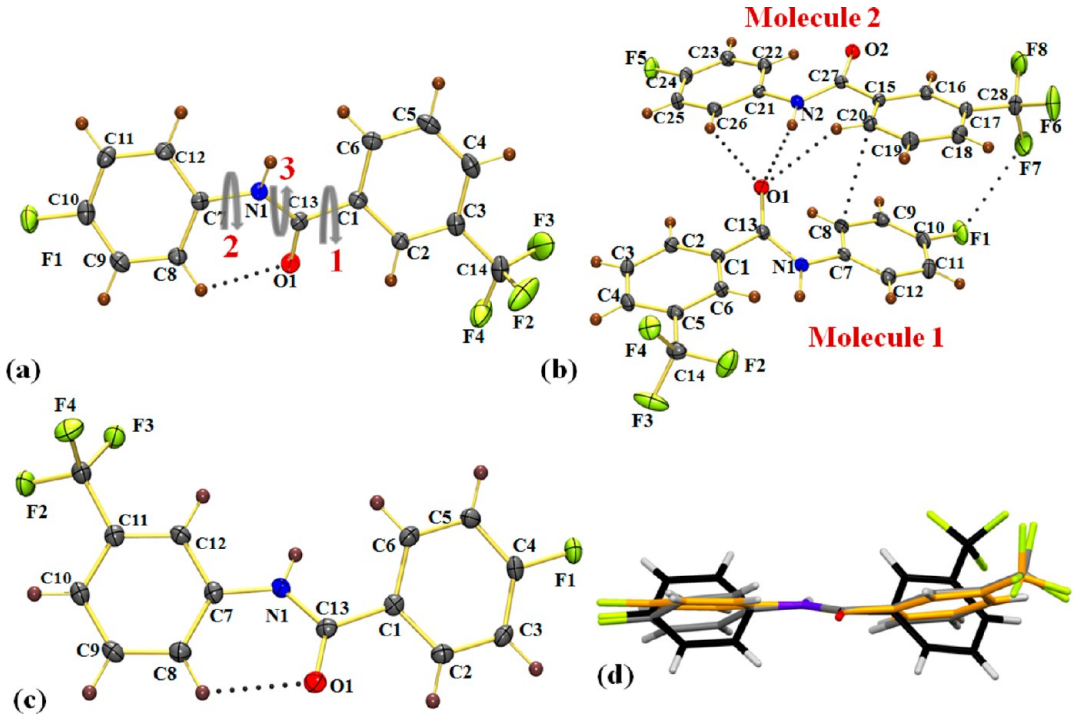

Figure 6. ORTEP of (a) **A-1**, (b) **A-2**, and (c) **B**, drawn with 50% ellipsoidal probability with atom numbering scheme. (d) Molecular overlay (drawn with Mercury 3.0) of three molecules (two molecules in the asymmetric unit of **A-2**) in the two polymorphs at solid state geometry. Color code for C atoms in figure: Gray for **A-1**, Black for **A-2** molecule 1, and Orange for **A-2** molecule 2.

Table 2. List of Selected Torsion Angles (deg) (gray arrows in Figure 6a) in A-1, A-2, and B

	Torsion 1[a] (deg) C2−C1−C13−N1	Torsion 2[a] (deg) C13−N1−C7−C12	Torsion 3[a] (deg) C7−N1−C13−C1
A-1	153.8(2)	−149.5(2)	175.9(2)
A-2	−136.6(1)/158.3(1)′	148.0(1)/168.7(1)′	173.9(1)/−178.8(1)′
B	−150.7(1)	162.0(1)	−176.0(1)

[a](′) for a second molecule in the asymmetric unit.

Table 3. Lattice Energy (kcal/mol) Partitioned into Coulombic, Polarization, Dispersion, and Repulsion Contribution by PIXEL Method

	comp. code	E_{Coul}	E_{Pol}	E_{Disp}	E_{Rep}	E_{Tot}[a]
1.	**A-1**	−16.2	−7.6	−30.3	24.4	−29.7
2.	**A-2**	−16.0	−6.5	−31.1	25.1	−28.4
3.	**B**	−15.6	−6.3	−32.2	24.4	−29.7

[a]Experimental sublimation energy reported for benzanilide[34] is 125.4 kJ/mol (29.95 kcal/mol).

Mata and co-workers have used equation (ii) in the estimation of the interaction energy of the gas phase complexes of R—H···FH (R = H, Li, Al, Cl, C≡CH) in the presence of an external electric field.[28a] The values for the interaction energies of the hydrogen bond were observed in the range of 3 < I.E < 90 kJ/mol.[28b] These equations were also extensively explored for different intermolecular interactions or contacts in the analysis of the crystal structure of picolinic acid N-oxide.[29] To the best of our knowledge, there is no report on the application of these equations for the estimation of interaction energies for weak C—H···F—C hydrogen bonds in molecular crystals. These equations were also found to be of importance in calculating the interaction energy of different intermolecular interactions when present in a given molecular pair in the crystal packing. Keeping in mind that

dx.doi.org/10.1021/cg5004758 | Cryst. Growth Des. XXXX, XXX, XXX−XXX

Table 4. Intra- and Intermolecular Interactions along with Interaction Energies (I.E.) Obtained from PIXEL Method[a]

motifs	symmetry code	centroid-centroid distance (Å)	E_{Coul}	E_{Pol}	E_{Disp}	E_{Rep}	E_{Tot}	selected involved interactions[b]	geometry (Å/ °)
				A-1 ($Pna2_1$, Z = 4)					
I	$x-1/2, -y+3/2, z$	5.300	−11.0	4.5	−12.0	15.4	−12.1	N1—H1···O1,	1.86, 157
								C6—H6···O1,	2.69, 125
								C12—H12···O1	2.64, 117
								$\pi\cdots\pi$ (C6···C8)	3.330(2)/3.684(2)[c]
								C10—F1···F2—C14	3.066(2), 109(1), 105(1)
II	$x, -y+1, z-1/2$	6.517	−2.2	−0.6	−5.5	2.5	−5.8	C2—H2···π (C5)	2.82, 139/3.44, 117[c]
III	$x, -y+2, z-1/2$	10.402	−1.6	−0.6	−3.5	2.0	−3.7	C12—H12···π (C9)	2.80, 132/3.55, 114[c]
IV	$-x-1/2, y-1/2, z+1/2$	9.865	−0.9	−0.6	−2.6	1.9	−2.2	C5—H5···π (C11)	2.66, 169/3.15, 154[c]
V	$-x+1/2, y+1/2, z-1/2$	9.300	−0.2	−0.5	−3.2	1.8	−2.1	C9—H9···π (C2)	2.70, 164/3.16, 168[c]
VI	$x, y+1, z$	13.699	0.0	−0.2	−1.6	0.8	−1.0	C11—H11···F2	2.61, 137
				A-2 (Cc, Z = 8)					
	1···2/2···1								
I	x, y, z	5.902	−11.3	−4.5	−10.6	14.2	−12.2	N2—H2N···O1,	1.89, 158
								C20—H20···O1,	2.56, 134
								C26—H26···O1	2.36, 132
								$\pi\cdots\pi$ (C8···C20)	3.561(2)/3.773(2)[c]
II	$x-1/2, y-1/2, z$	3.765	−11.4	−4.6	−12.7	16.2	−12.4	N1—H1N···O2	1.82, 155
								$\pi\cdots\pi$ (C5···C21)	3.463(2)/3.749(2)[c]
III	$x, y-1, z$	9.712	−2.5	−0.7	−4.0	2.9	−4.3	C6—H6···F5,	2.32, 162
								C12—H12···F5	2.65, 131
IV	$x+1/2, -y+1/2, z-1/2$	7.189	−1.0	−0.8	−6.0	3.7	−4.1	C22—H22···F4,	2.53, 141
								C16—H16···π (C3)	2.77, 127
V	$x-1/2, y+1/2, z$	9.167	0.0	−0.4	−3.1	1.5	−2.0	C8—H8···F6	2.41, 130
VI	$x, -y, z+1/2$	10.982	−0.6	−0.4	−1.9	1.3	−1.6	C19—H19···F1,	2.50, 122
								C20—H20···F1	2.57, 119
VII	$x-1/2, -y-1/2, z+1/2$	11.189	−0.4	−0.1	−1.2	0.3	−1.4	C14—F2···F7—C28	3.111(2), 137(1), 108(1)
VIII	$x, -y+1, z-1/2$	13.284	0.1	−0.1	−1.4	0.3	−1.0	C10—F1···F5—C24	3.121(2), 99(1), 114(1)
	1···1								
IX	$x, -y, z+1/2$	7.443	−1.4	−0.5	−6.5	3.8	−4.7	$\pi\cdots\pi$ (C1···C11)	3.428(2)/3.954(2)[c]
X	$x+1/2, -y-1/2, z-1/2$	12.364	−0.5	−0.1	−0.9	0.5	−1.0	C11—H11···F3	2.51, 158
	2···2								
XI	$x+1/2, y-1/2, z$	9.127	0.6	−0.4	−4.9	2.4	−2.4	$\pi\cdots\pi$ (C17···C25)	3.536(2)/4.242(2)[c]
XII	$x-1/2, -y+1/2, z+1/2$	10.911	−1.1	−0.2	−1.6	1.0	−2.0	C25—H25···F7	2.46, 148
				B ($P2_1/c$, Z = 4)					
I	$x, -y+3/2, z-1/2$	5.027	−9.9	−3.8	−11.7	13.8	−11.7	N1—H1···O1,	1.92, 149
								$\pi\cdots\pi$ (Cg1···Cg2)	3.603(1)
II	$-x+2, -y+1, -z+2$	6.678	−0.7	−0.5	−7.8	4.3	−4.7	$\pi\cdots\pi$ (C10···C12)	3.540(1)
III	$-x+1, y-1/2, -z+3/2$	9.057	−2.7	−1.0	−4.4	3.5	−4.7	C6—H6···F1,	2.23, 174
								C12—H12···F1	2.56, 131
IV	$-x+2, y-1/2, -z+5/2$	9.409	−1.2	−0.6	−3.7	2.1	−3.4	C8—H8···F2,	2.52, 126
								C10—H10···O1	2.70, 127
V	$-x+1, -y+2, -z+2$	10.131	0.1	−0.4	−5.3	3.2	−2.3	$\pi\cdots\pi$ (C2···C4)	3.527(1)
VI	$x, y+1, z$	12.496	−0.6	−0.1	−1.2	0.4	−1.5	C3—H3···F4	2.66, 137
VII	$x, -y+1/2, z-1/2$	10.995	−0.2	−0.1	−1.4	0.4	−1.3	C14—F3···F4—C14	2.926(1), 153(1), 106(1)

[a]Neutron values are given for all D—H···A interactions. [b]Only selected interactions have been listed. There may be other atom−atom contacts. The full lists are given in Table S3 as obtained after QTAIM analysis. [c]Geometry from centroid of the related ring for the corresponding interaction.

the study of intermolecular interactions in terms of evaluation of the interaction energies for the cluster of molecules (dimer, trimer, etc.) has limitations when multiple intermolecular interactions are present, we believe that the present approach is the most significant. The results of the topological analysis on the different molecular pairs are presented in Supporting Information Table S3. The graphics were plotted by program suit AIMStudio (v 13.05.06).

Unit Conversion Relations, Used in the Work.

(1) Distance: 1 au = 1 bohr = 0.5292 Å.
(2) Electron density: 1 au = 1 e/bohr^3 = 6.748 e/Å^3.
(3) Laplacian ($\nabla^2\rho$): 1 au = 1 e/bohr^5 = 24.098 e/Å^5.
(4) Energy: 1 au = 627.529 kcal/mol.

Electrostatic Potential Map on the Hirshfeld Surface. For visualizing and analyzing intermolecular interactions in molecular crystals (particularly for the polymorphs), the graphical tool, Hirshfeld surfaces mapped with different properties were found to be very much useful.[30] Molecular Hirshfeld surfaces represent an isosurface (constructed by the program Crystal explore 3.0[31]) where the electron distribution of a sum of spherical atoms for the molecule

dx.doi.org/10.1021/cg5004758 | Cryst. Growth Des. XXXX, XXX, XXX−XXX

(the promolecule) dominates the corresponding sum over the crystal (the procrystal).

In the current work, the electrostatic potentials (ESP) was mapped on the Hirshfeld surfaces[32] for **A-1**, two molecules in **A-2** and **B** over the range −0.03 au (red) through 0.0 (white) to 0.03 au (blue). For this purpose *ab initio* wave functions for all the molecules were calculated at HF/6-31G** by the Gaussian program. The results are shown in Supporting Information Figure S5 and Figures 7d−e.

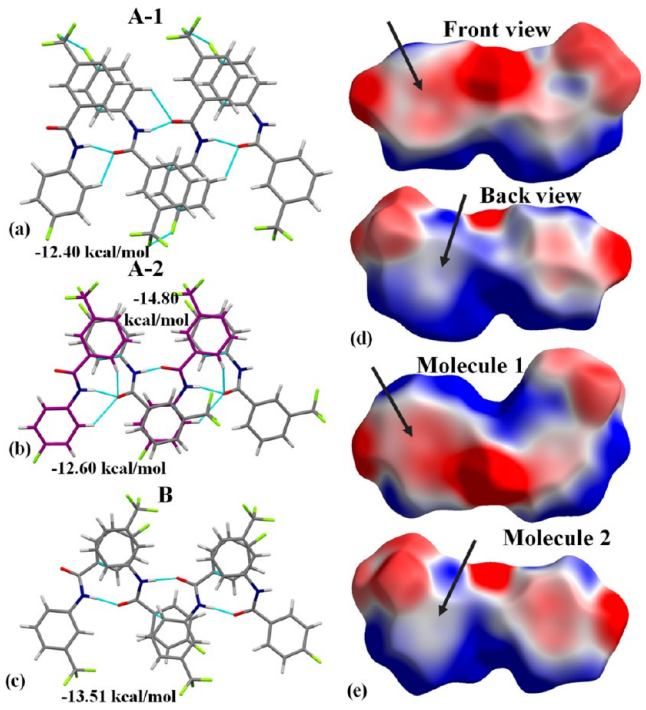

Figure 7. Common molecular chain in (a) **A-1**, (b) **A-2**, and (c) **B** via strong N—H···O═C, weak C—H···O═C hydrogen bonds along with $\pi\cdots\pi$ interactions. Electrostatic potential (ESP) mapped on the Hirshfeld surface of (d) **A-1** and (e) **A-2** (two molecules), over the range −0.03 au (red) through 0.0 (white) to 0.03 au (blue). The marked arrows show the Ph-rings which are involved in $\pi\cdots\pi$ stacking interactions with N—H···O═C H-bond.

RESULT AND DISCUSSIONS

ORTEPs of two polymorphs of A (**A-1** and **A-2**) and **B** are presented in Figure 6. It is to be noted that **A-1** and **A-2** contain one and two molecules in the asymmetric unit, respectively. The two molecules in the asymmetric unit in **A-2** have differences in the orientation of the $-CF_3$ group with respect to the C═O bond. In molecule 1, the two were present antiparallel to each other, while in molecule 2, opposite orientations (similar as in **A-1**) was observed (Figure 6), with the difference in corresponding torsion angle (torsion 1, Table 2) being 109°. These conformational differences associated with the molecules of the polymorphs were clearly depicted in Figure 6d. It is to be mentioned here that the crystal of **A-1** was obtained from the bulk material (representing mainly **A-2**, Figure 5) after heating in benzene (70 °C) followed by crystallization at RT, whereas crystallization at LT (5 °C, in benzene) resulted only in **A-2** (Table S1, Figure 1).

The primary recognition motif in **A-1** and **A-2**, consisting of N—H···O═C hydrogen bond and $\pi\cdots\pi$ interactions, is reminiscent of the cooperativity that exists in the crystal structure of DNA. Similar packing motif (molecular chain) is also present in **B** (Figure 7). It is to be noted that the zigzag molecular chain via N—H···O═C and $\pi\cdots\pi$ interactions is rare in the crystal packing of these class of compounds. The previous reports on fluorine substituted[8a] and other halogen substituted benzanilides[8b] including the parent compound (ref code in CSD: BZANIL01) do not show the formation of such molecular chains via N—H···O═C hydrogen bond. The possible reason could be the presence of the two phenyl rings in different electronic environment due to the presence of fluorine and trifluoromethyl ($-CF_3$) groups. The electrostatic potential mapped on the Hirshfeld surface[32] displays the presence of complementary electrostatic regions (electropositive or electronegative, marked with arrow in Figure 7d,e) involving the phenyl rings in parallel orientation, resulting in $\pi\cdots\pi$ interactions, which stabilize the molecular chain. Although the basic structural motif was observed to be similar in all three cases, the 3D-arrangement of the molecules in their crystal packing is entirely different (Figure 8−10). The main difference

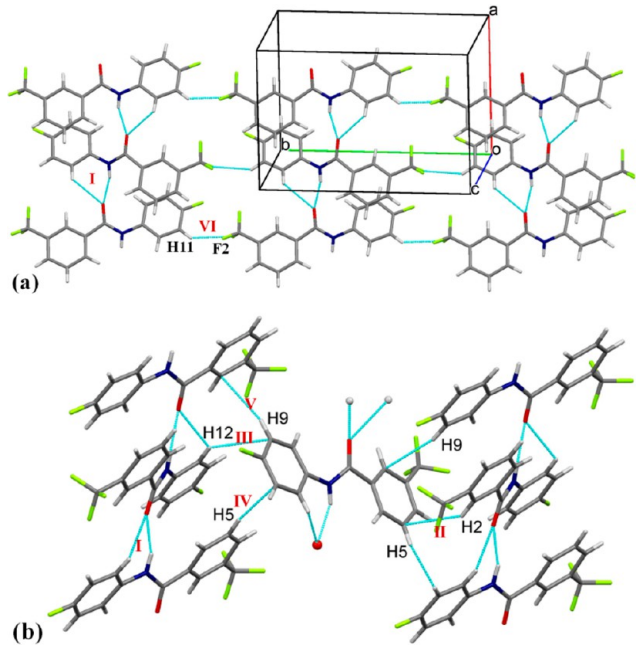

Figure 8. (a) Packing of molecules in **A-1** down the *ab* crystallographic plane via strong N—H···O═C and weak C—H···O═C and C—H···F—C (sp^3) hydrogen bonds. The Roman numerals indicate molecular motifs, presented in Table 4. (b) Part of crystal packing in **A-1** displaying network of the strong N—H···O═C and weak C—H···O═C and C—H···π hydrogen bonds. The Roman numerals indicate molecular motifs, presented in Table 4.

in the two polymorphs of **A-1** and **A-2** appears in the nature of the weaker interactions. In the case of the former, it is mainly the weak C—H···π interactions (Figure 8b) which were observed to stabilize the crystal packing along with only one C—H···F interaction (2.61 Å/137°, Table 4, Figure 8a), the distance being less than the sum of the van der Waals radii (2.67 Å) of hydrogen and fluorine.[33] In the case of the latter, it is mainly the weak C—H···F's along with $\pi\cdots\pi$ and C—F···F—C that stabilize the crystal packing (Figure 9). It is to be noted that out of the 8 fluorine atoms in the asymmetric unit of **A-2**, six are involved in the formation of short C—H···F interactions (including the one with H···F distance being 2.32 Å and directionality of 162°, Table 4). Furthermore, compound **B**, involves the network of weak C—H···O═C, C—H···F—C(sp^2/sp^3) interactions resulting in

dx.doi.org/10.1021/cg5004758 | *Cryst. Growth Des.* XXXX, XXX, XXX−XXX

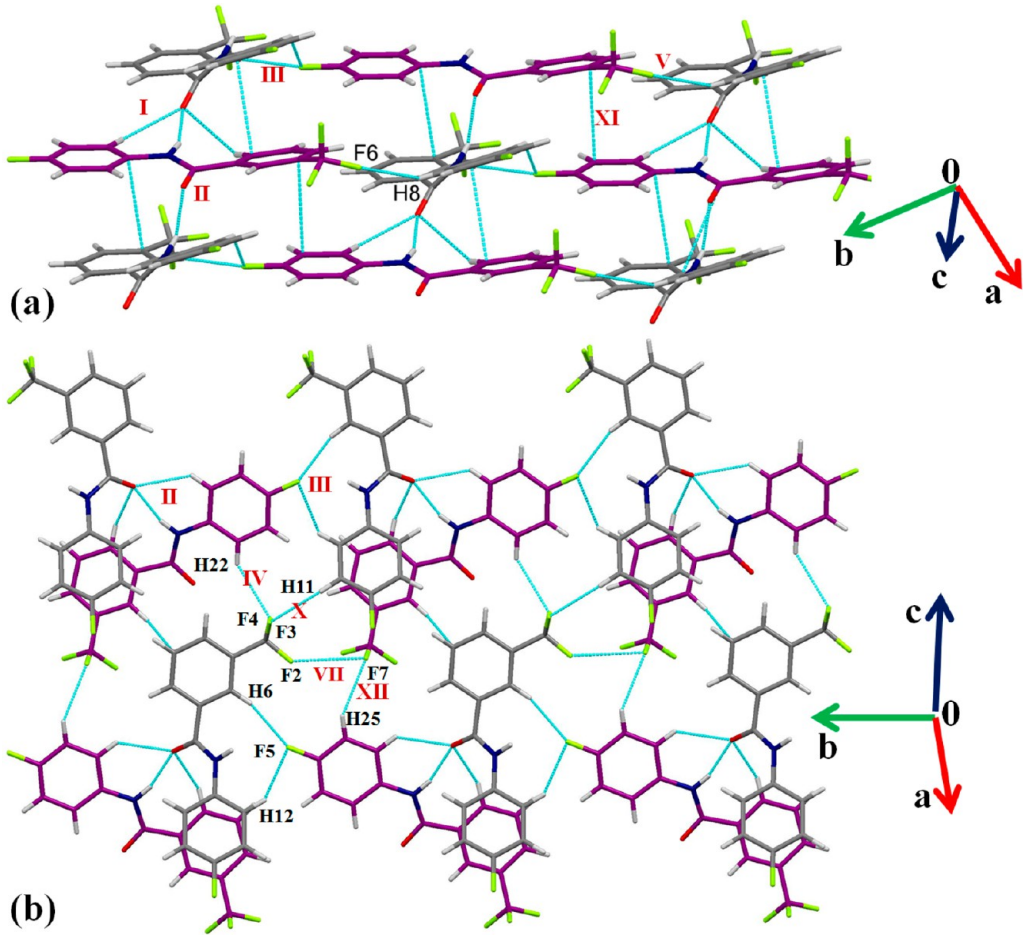

Figure 9. (a) Packing of molecules in **A-2** via the network of strong N—H···O═C and weak C—H···O═C, C—H···F—C(sp^2), and C—H···F—C(sp^3) hydrogen bonds along with $\pi\cdots\pi$ interactions. (b) Packing of molecules in **A-2** via the network of strong N—H···O═C and weak C—H···O═C, C—H···F—C(sp^2), and C—H···F—C(sp^3) hydrogen bonds along with C(sp^3)—F···F—C(sp^3) interactions. The Roman numerals indicate molecular motifs, presented in Table 4.

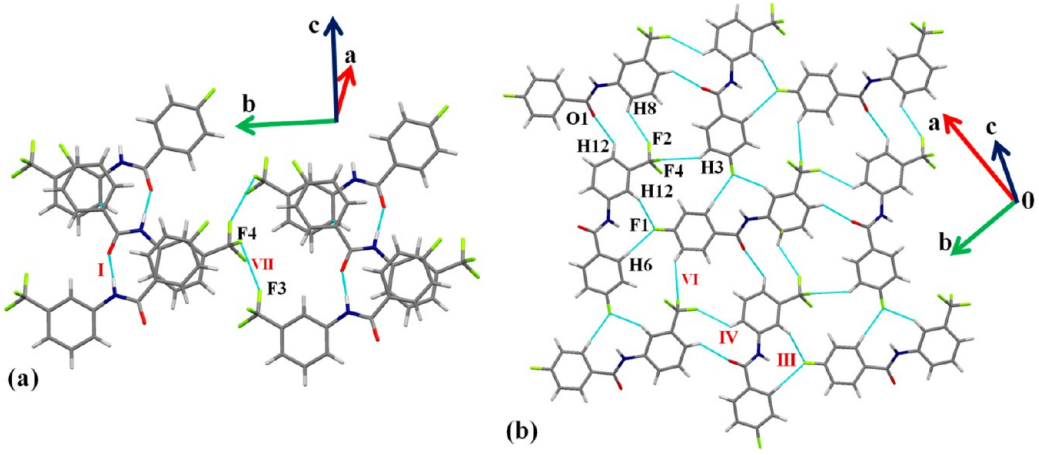

Figure 10. (a) Packing of molecules in **B** via the network of strong N—H···O═C hydrogen bonds along with $\pi\cdots\pi$ and C(sp^3)—F···F—C(sp^3) interactions. (b) Formation of herringbone sheet in **B** via the network of weak C—H···O═C, C—H···F—C(sp^2), and C—H···F—C(sp^3) hydrogen bonds. The Roman numerals indicate molecular motifs, presented in Table 4.

the formation of a herringbone sheet in the crystal packing down the *ab* crystallographic plane (Figure 10).

Lattice energy calculations with the PIXEL method[20] shows that **A-1** is 1.3 kcal/mol more stable than **A-2** (Table 3). Compound **B** was observed to have similar lattice energy (29.7 kcal/mol, comparable with the experimental sublimation energy of benzanilide[34]) as **A-1**. The intermolecular interaction energies for the different dimers (extracted from the crystal packing) in **A-1**, **A-2**, and **B** were also determined using PIXEL method (Table 4). In all three crystal structures, the molecular pair consists of a strong N—H···O═C hydrogen bond (motif I, Table 4) and were observed to provide similar stabilization

dx.doi.org/10.1021/cg5004758 | *Cryst. Growth Des.* XXXX, XXX, XXX−XXX

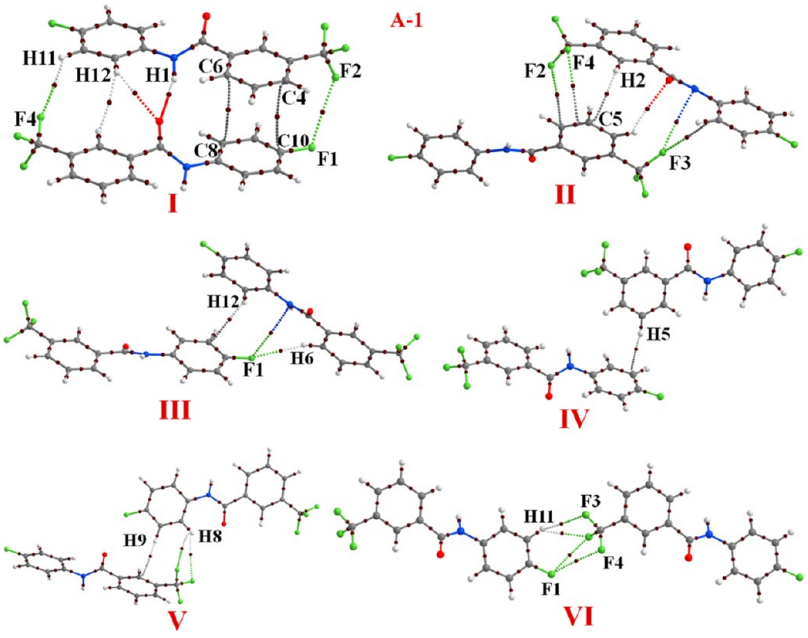

Figure 11. Selected molecular pairs **A-1**. The small brown spheres indicate the bond critical points (BCPs).

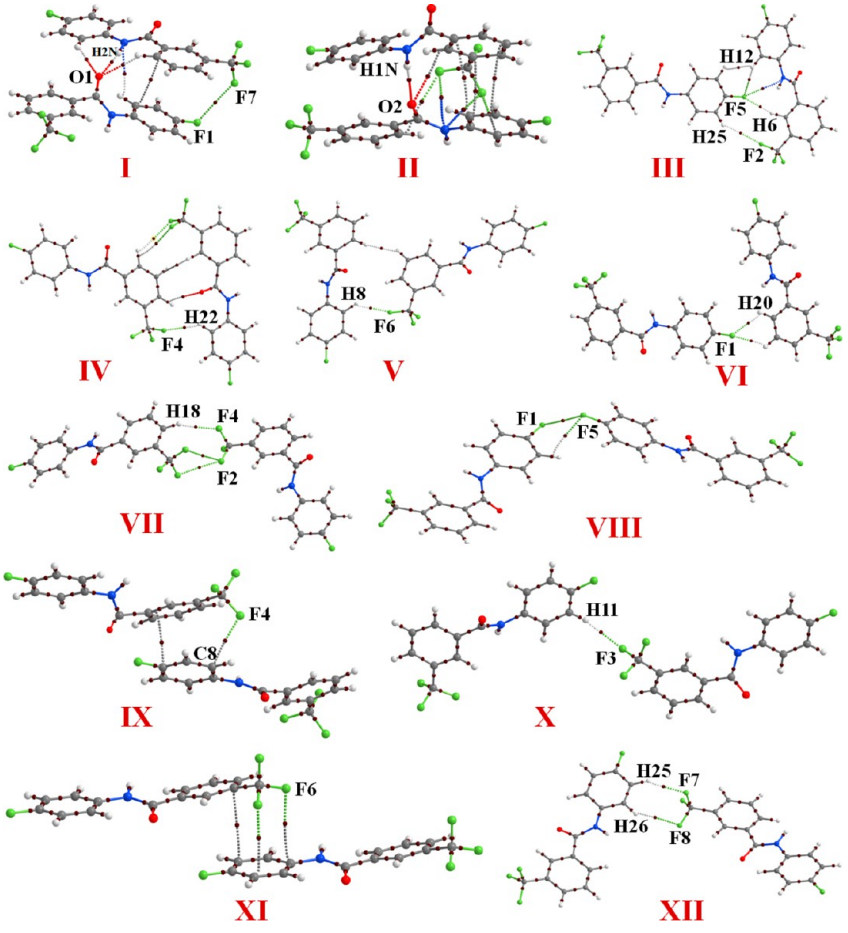

Figure 12. Selected molecular pairs in **A-2**. The small brown spheres indicate the bond critical points (BCPs).

(I.E. ≈ 12 kcal/mol with Coulombic contribution of 39−43%) toward the crystal packing. It is of interest to observe that the highly acidic hydrogens (H6 with F5 in **A-2** and H6 and H12 with F1 in **B**, motif III's) are involved in the formation of a short C—H···F in **A-2** and **B**, the interaction energy having a substantial Coulombic contribution (35% in **A-2** and 34% in **B**) in comparison to the other weak interactions which are primarily of a dispersive character.

The complete representation of the intramolecular and intermolecular bond critical points (theory of atoms-in-molecules

dx.doi.org/10.1021/cg5004758 | *Cryst. Growth Des.* XXXX, XXX, XXX−XXX

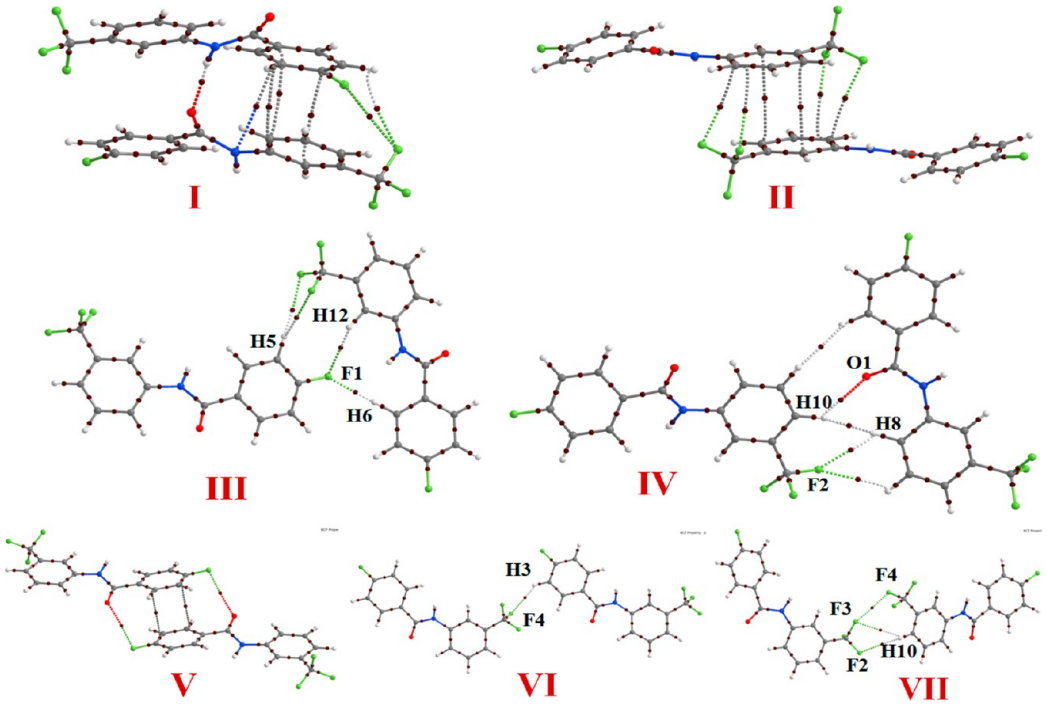

Figure 13. Selected molecular pairs with their interaction energies in **B**. The small brown spheres indicate the bond critical points (BCPs).

(AIM)[26]) for the different crucial dimeric motifs (Table S3) which govern crystal formation are shown in Figures 11−13. Multiple (3,−1) BCPs were observed between most of the molecular pairs which indicate the existence of intermolecular contacts between the atoms connecting the molecules. Hence the characterization of individual intermolecular interactions become difficult with traditional *ab initio* quantum mechanical methods as was also mentioned in the section on theoretical calculation. According to the theory of QTAIM, the BCP is a region on the bond path where the electron density, $\rho(r)$, is minimum along the bond path and maximum in the perpendicular plane, and thus $\nabla\cdot\rho(r) = 0$. The Laplacian ($\nabla^2\rho$) indicates the region where $\rho(r)$ is locally concentrated ($\nabla^2\rho < 0$) or depleted ($\nabla^2\rho > 0$). For closed-shell interactions, such as hydrogen bond, the Laplacian ($\nabla^2\rho$) at BCP is positive.

For a strong N—H···O hydrogen bond, the electron density, $\rho(r)$, and the Laplacian ($\nabla^2\rho$) were observed between 0.162−0.198 e/Å^3 and 2.400−2.722 e/Å^5, respectively, for the H···O bond path distances (R_{ij}) which lie between 1.861 and 1.962 Å. The calculated dissociation energy for the N—H···O hydrogen bond ranges 6−8 kcal/mol as obtained from equations (i) and (ii) (see Supporting Information section on Theoretical calculation, Table S3). Along with the strong N—H···O hydrogen bond, (3, −1) bond critical points (BCPs) for the weak interactions like C—H···O, C—H···C (π), C—H···F, C···C (π), C—F···C(π), and C—F···F—C were also observed in the crystal packing (Figures 11−13). These are presented in Supporting Information Table S3 with their topological parameters. In case of **A-1**, there are (3,−1) bond critical points (BCP) for C—H···C (π) interactions observed in motifs II, III, IV, and V (Figure 11). There is only one BCP observed for a C—H···F interaction (involving H11 with F2) at a distance shorter than the sum of their van der Waals radii[33] in motif VI along with other C—H···F (involving H11 with F3; d = 2.80 Å) and C—F···F—C interactions. The C—F···F—C contact is a closed-shell interaction and also ubiquitious in fluorine containing molecules, and these have been well characterized in the literature.[35] Furthermore, it is to be mentioned that in the block form (**A-2**) there are 8 BCPs for C—H···F interactions at distances shorter than the sum of their van der Waals radii observed in different molecular motifs (Figure 12, Supporting Information Table S3). The topological parameters and dissociation energies for the selected C—H···F interactions in **A-1**, **A-2**, and **B** are presented in Table 5. The topological analysis reveals the magnitude of the electron density to be 0.063e/Å^3 for the short C—H···F interaction in **A-2**, the interaction energy being −2.15 kcal/mol (Motif III, Table 5). This is absent in **A-1**. There are related short C—H···F H-bonds in the crystal packing involving different hydrogens with the fluorine atoms (connected to trifluoromethyl group, the electron density for the BCPs are in the range of 0.04−0.05e/Å^3, the corresponding stabilization energies are in the range of 1.4−1.9 kcal/mol). Following these observations, it is noteworthy that the crystal structure of **B**, which is an isomeric variant of **A**, contains the same dimeric motif III, as is present in **A-2** (Figure 14). The key feature in the crystal structure of **B**, consists of a short and nearly linear C—H···F (2.23 Å/172°), an observation which is extremely rare in crystal structures with organic fluorine, particularly when strong intermolecular N—H···O═C H-bonds and several weak C—H···π and π···π interactions are present (Table 4 and Supporting Information Table S3). The electron density at the critical point is 0.084e/Å^3 and the interaction energy is −2.89 kcal/mol (Table 5). These values for the stabilization energy are relatively high, considering the value reported by Novoa (the interaction energy was 0.53 kcal/mol (from ab initio calculations), who performed an in-depth study on fluorine containing compounds in different electronic environments.[36]

The CSD search[37] for the existence of generalized C—H···F—C contacts, the distance being less than 2.30 Å and the directionality greater than 165°, resulted in 19 hits (Supporting

dx.doi.org/10.1021/cg5004758 | *Cryst. Growth Des.* XXXX, XXX, XXX−XXX

Table 5. Selected C—H···F Interactions in A-1, A-2, and B along with Their Topological Parameters[a]

$d_{H\cdots F}$ (Å)[b]	R_{ij} (Å)	ρ_{BCP} (e/Å^3)	$\nabla^2\rho_{BCP}$ (e/Å^5)	V_b (a.u.)	G_b (a.u.)	D.E^V/ D.E^{Gc} (kcal/mol)	related motif in Tables 4 and S3
			A-1 (Plate)				
2.87	2.902	0.018	0.311	−0.001 895	0.002 561	0.59/0.69	I
2.72	2.739	0.027	0.400	−0.002 806	0.003 476	0.88/0.94	III
2.61	2.631	0.039	0.551	−0.004 027	0.004 869	1.26/1.31	VI
2.80	2.824	0.026	0.418	−0.002 673	0.003 503	0.84/0.94	
			A-2 (Block)				
2.32	2.340	0.063	0.867	−0.006 838	0.007 918	2.15/2.13	III
2.65	2.680	0.039	0.554	−0.004 090	0.004 831	1.28/1.30	
2.53	2.554	0.044	0.619	−0.004 589	0.005 503	1.44/1.48	IV
2.41	2.444	0.054	0.803	−0.006 056	0.007 195	1.90/1.94	V
2.50	2.537	0.046	0.710	−0.005 261	0.006 312	1.65/1.70	VI
2.57	2.607	0.045	0.659	−0.004 895	0.005 822	1.54/1.57	
2.70	2.725	0.029	0.432	−0.002 986	0.003 733	0.94/1.00	VII
2.51	2.526	0.044	0.602	−0.004 568	0.005 409	1.43/1.46	X
2.46	2.476	0.053	0.708	−0.005 556	0.006 453	1.74/1.73	XII
			B				
2.23	2.244	0.084	1.118	−0.009 207	0.010 402	2.89/2.80	III
2.56	2.593	0.046	0.642	−0.004 884	0.005 772	1.53/1.55	
2.78	2.811	0.026	0.410	−0.002 668	0.003 460	0.84/0.93	
2.89	2.916	0.020	0.305	−0.001 820	0.002 491	0.57/0.67	
2.52	2.561	0.045	0.677	−0.004 986	0.006 004	1.56/1.62	IV
2.75	2.816	0.028	0.461	−0.003 019	0.003 900	0.95/1.05	
2.66	2.685	0.034	0.495	−0.003 489	0.004 311	1.09/1.16	VI
2.91	2.957	0.020	0.338	−0.001 989	0.002 747	0.62/0.74	VII

[a]The complete lists are given in Table S3. [b]$d_{H\cdots F}$ = crystallographic H···F interaction distances from Table S3. [c]D.E^V = 0.5 V_b; D.E^G = 0.429G_b; V_b and G_b are local potential energy and kinetic energy density at the bond critical points (BCP), respectively. Interaction energy (I.E) = −D.E.

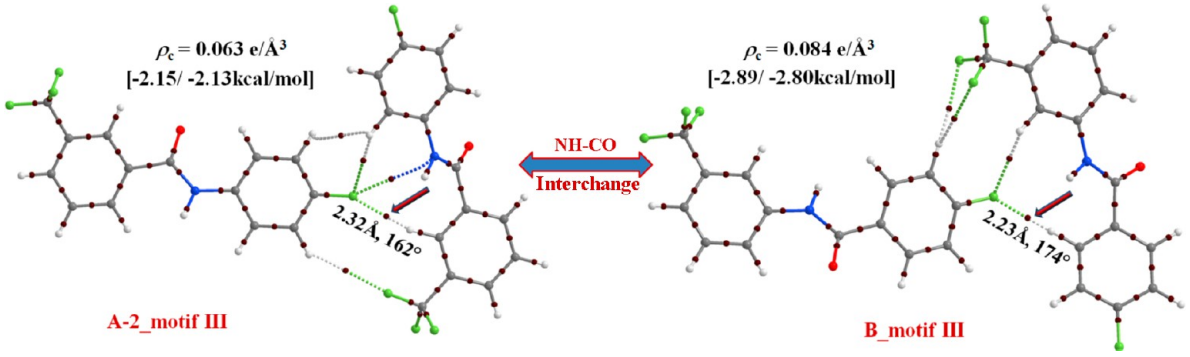

Figure 14. Similar molecular motif in **A-2** and **B**, displaying short C—H···F hydrogen bonds (marked with arrows) with other interactions. Bond critical points are shown with brown spheres.

Information section S4). Out of these, 12 compounds (having a maximum of one fluorine atom in terms of their electronic environment) were selected for a full topological analysis (Supporting Information Table S4 and Figure S6). It was observed that only for three compounds, ref codes NIZVAU02, JEFCIH, and LUHCEX, the H···F contact distance was observed to be less than our reported value of 2.23 Å. The geometry (neutron corrected) of the C—H···F interaction in these is 2.13 Å /174°, 2.14 Å /171°, and 2.22 Å /174°, respectively. The electron densities at the BCP and interaction energy were observed to be 0.094 e/Å^3 /3.41 kcal/mol, 0.099 e/Å^3/ 3.57 kcal/mol, and 0.074 e/Å^3 /2.60 kcal/mol, respectively. It is of interest to note that the highest stabilized C—H···F interaction in NIZVAU02 consists of a conformationally rigid molecule, while the second one, JEFCIH, does not possess any strong hydrogen bond donor. The conformationally flexible molecule LUHCEX has a similar stabilization when compared with **B** (the geometrical parameters for C—H···F interaction being similar to **B**).

The dependence of the electron density (ρ) at BCP for all reported C—H···F interactions [42 data points from a total of 15 crystal structures, including 12 from CSD, Supporting Information Tables S3 and S4] and its dissociation energy with H···F bond path distances (Figure 15) depict the exponential dependence with the latter. For the range between 2.1 and 3.1 (Å) ($r_{H\cdots F}$), the variation of electron density at BCP and the dissociation energy[17] shows the inverse dependence with the H···F distances, and these lie in the ranges 0.095 > ρ_{BCP} > 0.015 (e/Å^3) and 3.5 > D.E$_{H\cdots F}$ > 0.40 (kcal/mol). Fitting of scattered plot of dissociation energy (D.E) vs crystallographic H···F interaction distances ($d_{H\cdots F}$) (Figure 15c) also shows exponential decrease of D.E with increase of $d_{H\cdots F}$. The values of electron density and Laplacian of the electron density at the

dx.doi.org/10.1021/cg5004758 | Cryst. Growth Des. XXXX, XXX, XXX−XXX

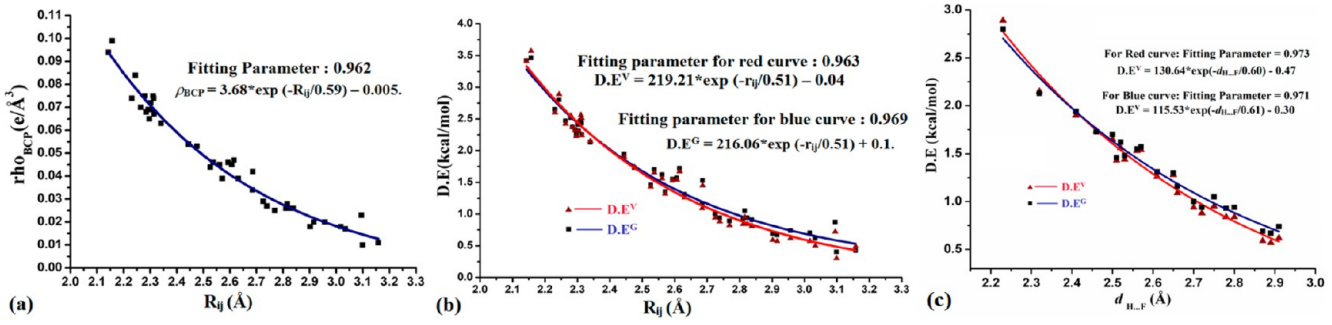

Figure 15. (a) Variation of the electron density (ρ_{BCP}) at BCP vs H···F-bond path distance (R_{ij}). (b) Variation of the dissociation energies (D.E) vs R_{ij}. (c) Variation of the dissociation energies (D.E) vs crystallographic distances ($d_{H\cdots F}$).

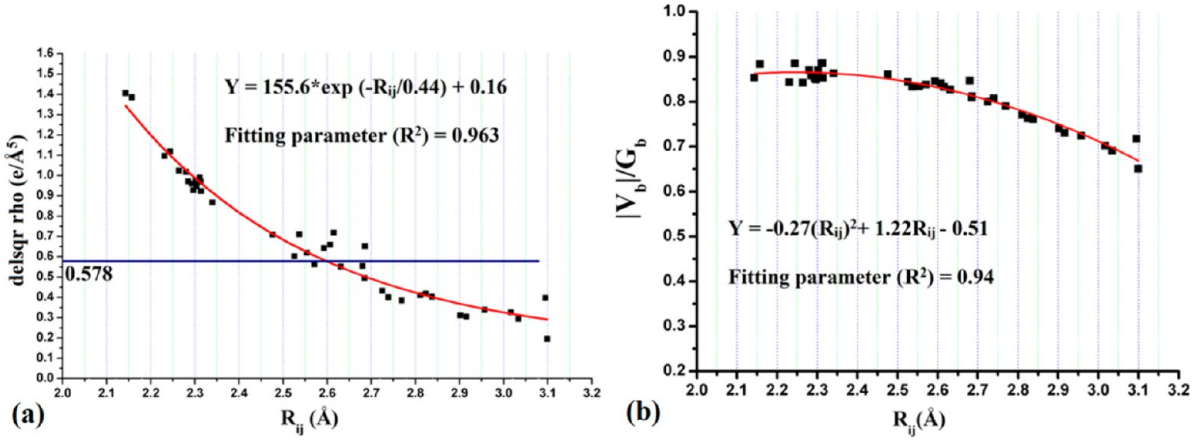

Figure 16. (a) Variation of Laplacian ($\nabla^2\rho$) with R_{ij}. The solid red line is an exponential fit of the data points. The solid blue line at $\nabla^2\rho$ = 0.578 e/Å^5 is showing the minima in accordance with Popelier's criteria for existence of a H-bond (0.578 e/Å^5 < $\nabla^2\rho$ < 3.350 e/Å^5). (b) Variation of $|V_b|/G_b$ with R_{ij}. The solid red line is a polynomial fit of the data points.

BCP for C—H···F were observed to be comparable with those recently reported by Kaur and Choudhury.[38]

The Laplacian of the electron density [$\nabla^2\rho$ (e/Å^5)] was observed to be positive in all the ranges in R_{ij}[(Figure 16a) indicating the closed-shell character for these interactions.[11,28] In accordance with the Koch and Popelier criteria,[11b,39] the range of Laplacian values [0.578 < $\nabla^2\rho$ (e/Å^5) < 3.350] indicates the presence of an "H-bond" to fluorine, particularly applicable for short C—H···F distances ($d_{H\cdots F}$ < 2.67, Figure 16a). Furthermore, it is observed that this criterion for $d_{H\cdots F}$ near 2.7 Å appears unpredictable and does not hold well for longer C—H···F distances, as also observed in the recent literature.[40]

It is to be noted that the value of $|V_b|/G_b$ < 1 (criteria for H-bond as suggested by Espinosa[41]) for all ranges in R_{ij} for H···F interactions (Figure 16b).

In accordance, with the definition of a H-bond, as defined in IUPAC,[42] three very important criteria deserve special mention with respect to this study. The first one is the "cooperativity observed in hydrogen bonded framework", second the "directionality and the resultant influence on crystal packing", and the third the observation of a (3, −1) BCP between the donor and acceptor in the topological analysis of the ED are defined characteristics for the presence of a H-bond. In our study, with the "observation" of the above-mentioned criteria, the interaction between H and F is indeed a true "H-bond". The nature of the participating atoms (in terms of size and electronegativity) and the presence of other atoms in the molecule along with the crystal environment play a very significant role in deciding the energetics involved in such weak interactions. These results delineate the versatility of interactions involving organic fluorine. In the future, the methodology discussed above can be advanced to understand protein—ligand interactions in biomolecules wherein either of the components contain fluorine in their active site.

CONCLUSIONS

In conclusion, short and highly directional C—H···F interactions were observed in the presence of strong N—H···O═C in molecular crystals. These are not a consequence of crystal packing and have implications in the generation of polymorph in the solid state. Moreover, the acidic hydrogens were observed to be involved in the formation of a short C—H···F, the interaction energy having a substantial Coulombic contribution in comparison to the other weak interactions which are primarily of a dispersive character. A full crystallographic and topological analysis on these interactions does reveal new and convincing evidence to term short intermolecular contacts with organic fluorine as a true "hydrogen bond". The methodology described in this article will now be extended to understanding intermolecular interactions involving different donor types C(sp^2(nonaromatic), sp^3)—H, N—H, and O—H interacting with fluorine in different electronic environments.

ASSOCIATED CONTENT

Supporting Information

Details on synthesis, characterization, crystal growth, theoretical calculations, and CSD database search are provided. This

dx.doi.org/10.1021/cg5004758 | Cryst. Growth Des. XXXX, XXX, XXX−XXX

material is available free of charge via the Internet at http://pubs.acs.org.

AUTHOR INFORMATION

Corresponding Author

*Fax: 91-0755-6692370. E-mail: dchopra@iiserb.ac.in.

Notes

The authors declare no competing financial interest.

ACKNOWLEDGMENTS

P.P. thanks UGC-India for research scholarship. We acknowledge IISER Bhopal for research facilities and infrastructure. The authors also thank Prof T. N. Guru Row for data collection on the CCD facility at IISc, Bangalore under the IRHPA-DST Scheme. D.C. thanks DST-Fast Track Scheme for research funding.

REFERENCES

(1) (a) Philip, D.; Stoddart, J. F. *Angew. Chem., Int. Ed. Engl.* **1996**, *35*, 1154−1196. (b) Desiraju, G. R. *J. Am. Chem. Soc.* **2013**, *135*, 9952−9967. (c) Hunter, C. A. *Angew. Chem., Int. Ed.* **2004**, *43*, 5310−5324. (d) Schneider, H.-J. *Angew. Chem., Int. Ed.* **2009**, *48*, 3924−3977. (e) Dunitz, J. D.; Gavezzotti, A. *Chem. Soc. Rev.* **2009**, *38*, 2622−2633. (f) Cerny, J.; Hobza, P. *Phys. Chem. Chem. Phys.* **2007**, *9*, 5291−5303.

(2) Desiraju, G. R. *Angew. Chem., Int. Ed.* **2011**, *50*, 52−59.

(3) (a) Desiraju, G. R. *Chem. Commun.* **2005**, 2995−3001. (b) Bosch, E. *Cryst. Growth Des.* **2010**, *10*, 3808−3813. (c) Takahashi, O.; Kohno, Y.; Nishio, M. *Chem. Rev.* **2010**, *110*, 6049−6076. (d) Nishio, M. *Phys. Chem. Chem. Phys.* **2011**, *13*, 13873−13900. (e) Desiraju, G. R.; Steiner, T. *The Weak Hydrogen Bond in Structural Chemistry and Biology*; Oxford University Press: Oxford, 1999.

(4) Dunitz, J. D. *ChemBioChem* **2004**, *5*, 614−621.

(5) (a) Thalladi, V. R.; Weiss, H.-C.; Blaser, D.; Boese, R.; Nangia, A.; Desiraju, G. R. *J. Am. Chem. Soc.* **1998**, *120*, 8702−8710. (b) Thakur, T. S.; Kirchner, M. T.; Blaser, D.; Boese, R.; Desiraju, G. R. *CrystEngComm* **2010**, *12*, 2079−2085. (c) Parsch, J.; Engels, J. W. *J. Am. Chem. Soc.* **2002**, *124*, 5564−5672.

(6) (a) Berger, R.; Resnati, G.; Metrangolo, P.; Weber, E.; Hulliger, J. *Chem. Soc. Rev.* **2011**, *40*, 3496−3508. (b) Chopra, D.; Guru Row, T. N. *CrystEngComm* **2011**, *13*, 2175−2186. (c) Tressaud, A.; Haufe, G. *Fluorine and Health: Molecular Imaging, Biomedical Materials and Pharmaceuticals*; Elsevier: Amsterdam, 2008. (d) Schneider, H.-J. *Chem. Sci.* **2012**, *3*, 1381−1394.

(7) Choudhury, A. R.; Guru Row, T. N. *Cryst. Growth Des.* **2004**, *4*, 47−52.

(8) (a) Chopra, D.; Guru Row, T. N. *CrystEngComm* **2008**, *10*, 54−67. (b) Nayak, S. K.; Reddy, M. K.; Guru Row, T. N.; Chopra, D. *Cryst. Growth Des.* **2011**, *11*, 1578−1596. (c) Panini, P.; Chopra, D. *CrystEngComm* **2012**, *14*, 1972−1989. (a) Lee, H. Y.; Olasz, A.; Pink, M.; Park, H.; Lee, D. *Chem. Commun.* **2011**, *47*, 481−483. (b) Chopra, D.; Guru Row, T. N. *Cryst. Growth Des.* **2008**, *8*, 848−853.

(9) (a) Lee, H. Y.; Olasz, A.; Pink, M.; Park, H.; Lee, D. *Chem. Commun.* **2011**, *47*, 481−483. (b) Chopra, D.; Guru Row, T. N. *Cryst. Growth Des.* **2008**, *8*, 848−853.

(10) (a) Chopra, D.; Thiruvenkatam, V.; Guru Row, T. N. *Cryst. Growth Des.* **2006**, *6*, 843−845. (b) Chopra, D.; Thiruvenkatam, V.; Manjunath, S. G.; Guru Row, T. N. *Cryst. Growth Des.* **2007**, *7*, 868−874. (c) Vasylyeva, V.; Merz, K. *Cryst. Growth Des.* **2010**, *10*, 4250−4255. (e) Dikundwar, A. G.; Sathishkumar, R.; Guru Row, T. N.; Desiraju, G. R. *Cryst. Growth. Des.* **2011**, *11*, 3954−3963.

(11) (a) Bader, R. F. W. *Atoms in Molecules: A Quantum Theory*; Oxford University Press: Oxford, U.K., 1990. (b) Popelier, P. L *Atoms in Molecules: An Introduction*; Prentice Hall: London, 2000.

(12) Mueller, K.; Faeh, C.; Diederich, F. *Science* **2007**, *317*, 1881−1886.

(13) *CrystAlis CCD and CrystAlis RED*, v 1.171.33.31; Oxford Diffraction Ltd, Abingdon, Oxfordshire, England, 2009.

(14) Altomare, A.; Cascarano, G.; Giacovazzo, C.; Guagliardi, A. *J. Appl. Crystallogr.* **1993**, *26*, 343−350.

(15) Sheldrick, G. M. *Acta Crystallogr.* **2008**, *A64*, 112−122.

(16) Farrugia, L. J. WinGX, *J. Appl. Crystallogr.* **1999**, *32*, 837−838.

(17) Farrugia, L. J. *J. Appl. Crystallogr.* **1997**, *30*, 565.

(18) Macrae, C. F.; Bruno, I. J.; Chisholm, J. A.; Edgington, P. R.; McCabe, P.; Pidcock, E.; Rodriguez-Monge, L.; Taylor, R.; Streek, J.; Wood, P. A. *J. Appl. Crystallogr.* **2008**, *41*, 466−470, www.ccdc.cam.ac.uk/mercury.

(19) Petricek, V.; Dusek, M.; Palatinus, L. *JANA 2000*, 18/12/2007; Institute of Physics, Czech Republic, 2007; http://jana.fzu.cz.

(20) Gavezzotti, A. *New. J. Chem.* **2011**, *35*, 1360−1368.

(21) Frisch, M. J.; Trucks, G. W.; Schlegel, H. B.; Scuseria, G. E.; Robb, M. A.; Cheeseman, J. R.; Scalmani, G.; Barone, V.; Mennucci, B.; Petersson, G. A.; Nakatsuji, H.; Caricato, M.; Li, X.; Hratchian, H. P.; Izmaylov, A. F.; Bloino, J.; Zheng, G.; Sonnenberg, J. L.; Hada, M.; Ehara, M.; Toyota, K.; Fukuda, R.; Hasegawa, J.; Ishida, M.; Nakajima, T.; Honda, Y.; Kitao, O.; Nakai, H.; Vreven, T.; Montgomery, Jr., J. A.; Peralta, J. E.; Ogliaro, F.; Bearpark, M.; Heyd, J. J.; Brothers, E.; Kudin, K. N.; Staroverov, V. N.; Kobayashi, R.; Normand, J.; Raghavachari, K.; Rendell, A.; Burant, J. C.; Iyengar, S. S.; Tomasi, J.; Cossi, M.; Rega, N.; Millam, J. M.; Klene, M.; Knox, J. E.; Cross, J. B.; Bakken, V.; Adamo, C.; Jaramillo, J.; Gomperts, R.; Stratmann, R. E.; Yazyev, O.; Austin, A. J.; Cammi, R.; Pomelli, C.; Ochterski, J. W.; Martin, R. L.; Morokuma, K.; Zakrzewski, V. G.; Voth, G. A.; Salvador, P.; Dannenberg, J. J.; Dapprich, S.; Daniels, A. D.; Farkas, Ö.; Foresman, J. B.; Ortiz, J. V.; Cioslowski, J.; Fox, D. J. *Gaussian 09*, revision A.02; Gaussian, Inc., Wallingford, CT, 2009.

(22) Bernardi, F.; Boys, S. F. *Mol. Phys.* **1970**, *19*, 553−566.

(23) (a) Grimme, S.; Antony, J.; Ehrlich, S.; Krieg, H. *J. Chem. Phys.* **2010**, *132*, 154104−154119. (b) Moellemann, J.; Grimme, S. *Phys. Chem. Chem. Phys.* **2010**, *12*, 8500−8504. (c) Hujo, W.; Grimme, S. *Phys. Chem. Chem. Phys.* **2011**, *13*, 13942−13950. (d) Grimme, S. *J. Comput. Chem.* **2006**, *27*, 1787−1799.

(24) (a) Panini, P.; Mohan, T. P.; Gangwar, U.; Sankolli, R.; Chopra, D. *CrystEngComm* **2013**, *15*, 4549−4564. (b) Panini, P.; Chopra, D. *CrystEngComm* **2013**, *15*, 3711−3733.

(25) (a) Maschio, L.; Civalleri, B.; Ugliengo, P.; Gavezzotti, A. *J. Phys. Chem. A* **2011**, *115*, 11179−11186. (b) Dunitz, J. D.; Gavezzotti, A. *Cryst. Growth Des.* **2012**, *12*, 5873−5877. (c) Gavezzotti, A. *Mol. Phys.* **2008**, *106*, 1473−1485.

(26) Keith, T. A. *AIMALL*, version 13.05.06; TK Gristmill Software, Overland Park KS, USA, 2013; aim.tkgristmill.com.

(27) (a) Espinosa, E.; Molins, E.; Lecomte, C. *Chem. Phys. Lett.* **1998**, *285*, 170−173. (b) Lyssenko, K. A. *Mendeleev Commun.* **2012**, *22*, 1−7. (c) Borissova, A. O.; Korlyukov, A. A.; Antipin, M. Y.; Lyssenko, K. A. *J. Phys. Chem. A* **2008**, *112*, 11519−11522. (d) Vener, M. V.; Medvedev, A. G.; Churakov, A. V.; Prikhodchenko, P. V.; Tripol'skaya, T. A.; Lev, O. *J. Phys. Chem. A* **2011**, *115*, 13657−13663. (e) Wolstenholme, D. J.; Titah, J. T.; Che, F. N.; Traboulsee, K. T.; Flogeras, J.; McGrady, G. S. *J. Am. Chem. Soc.* **2011**, *133*, 16598−16604. (f) Wolstenholme, D. J.; Flogeras, J.; Che, F. N.; Decken, A.; McGrady, G. S. *J. Am. Chem. Soc.* **2013**, *135*, 2439−2442.

(28) (a) Mata, I.; Alkorta, I.; Espinosa, E.; Molins, E. *Chem. Phys. Lett.* **2011**, *507*, 185−189. (b) Vener, M. V.; Egorova, A. N.; Churakov, A. V.; Tsirelson, V. G. *J. Comput. Chem.* **2012**, *33*, 2303−2309.

(29) Shishkina, A. V.; Zhurov, V. V.; Stash, A. I.; Vener, M. V.; Pinkerton, A. A. *Cryst. Growth Des.* **2013**, *13*, 816−828.

(30) Spackman, M. A.; Jayatilaka, D. *CrystEngComm* **2009**, *11*, 19−32.

(31) Wolff, S. K.; Grimwood, D. J.; McKinnon, J. J.; Turner, M. J.; Jayatilaka, D.; Spackman, M. A. *CrystalExplorer*, version 3.0; University of Western Australia, 2012.

(32) Spackman, M. A.; McKinnon, J. J.; Jayatilaka, D. *CrystEngComm* **2008**, *10*, 377−388.

(33) Bondi, A. *J. Phys. Chem.* **1964**, *68*, 441−451.

(34) Umnahannant, P.; Chickos, J. *J. Chem. Eng. Data* **2012**, *57*, 1331−1337.
(35) (a) Chopra, D.; Cameron, T. S.; Ferrara, J. D.; Guru Row, T. N. *J. Phys. Chem. A* **2006**, *110*, 10465−10477. (b) Matta, C. F.; Castillo, N.; Boyd, R. J. *J. Phys. Chem. A* **2005**, *109*, 3669−3681. (c) Castillo, N.; Matta, C. F.; Boyd, R. J. *Chem. Phys. Lett.* **2005**, *409*, 265−269. (d) Castillo, N.; Matta, C. F.; Boyd, R. J. *J. Chem. Inf. Model.* **2005**, *45*, 354−359.
(36) D'Oria, E.; Novoa, J. J. *CrystEngComm* **2008**, *10*, 423−436.
(37) CSD version 5.34 updates (Nov 2012). The following constraints were applied: No REFCODE restrictions applied, 3D coordinates determined, *R* factor ≤ 0.1, No errors, Not polymeric, No ions, Only Organics containing only C, H, N, O, F elements.
(38) Kaur, G.; Choudhury, A. R. *Cryst. Growth Des.* **2014**, *14*, 1600−1616.
(39) Koch, U.; Popelier, P. L. A. *J. Phys. Chem.* **1995**, *99*, 9747−9754.
(40) Zhang, G.; He, W.; Chen, D. *Mol. Phys.* **2013**, DOI: 10.1080/00268976.2013.861085.
(41) (a) Mata, I.; Alkorta, I.; Molins, E.; Espinosa, E. *Chem.—Eur. J.* **2010**, *16*, 2442−2452. (b) Espinosa, E.; Alkorta, I.; Elguero, J.; Molins, E. *J. Chem. Phys.* **2002**, *117*, 5529−5542. (c) Espinosa, E.; Alkorta, I.; Rozas, I.; Elguero, J.; Molins, E. *Chem. Phys. Lett.* **2001**, *336*, 457−461.
(42) (a) Arunan, E.; Desiraju, G. R.; Klein, R. A.; Sadlej, J.; Scheiner, S.; Alkorta, I.; Clary, D. C.; Crabtree, R. H.; Dannenberg, J. J.; Hobza, P.; Kjaergaard, H. G.; Legon, A. C.; Mennucci, B.; Nesbitt, D. J. *Pure Appl. Chem.* **2011**, *83*, 1619−1636. (b) Arunan, E.; Desiraju, G. R.; Klein, R. A.; Sadlej, J.; Scheiner, S.; Alkorta, I.; Clary, D. C.; Crabtree, R. H.; Dannenberg, J. J.; Hobza, P.; Kjaergaard, H. G.; Legon, A. C.; Mennucci, B.; Nesbitt, D. J. *Pure Appl. Chem.* **2011**, *83*, 1637−1641.